Inorg. Chem. **2006**, *45*, 3588–3593

Syntheses, Structures, Ionic Conductivities, and Magnetic Properties of Three New Transition-Metal Borophosphates $Na_5(H_3O)\{M^{II}_3[B_3O_3(OH)]_3(PO_4)_6\}\cdot 2H_2O$ (M^{II} = Mn, Co, Ni)

Miao Yang, Jihong Yu,* Jiancheng Di, Jiyang Li, Peng Chen, Qianrong Fang, Yan Chen, and Ruren Xu

State Key Laboratory of Inorganic Synthesis and Preparative Chemistry, College of Chemistry, Jilin University, Changchun 130012, P.R. China

Received November 6, 2005

Three new open-framework transition-metal borophosphates $Na_5(H_3O)\{M^{II}_3[B_3O_3(OH)]_3(PO_4)_6\}\cdot 2H_2O$ (M^{II} = Mn, Co, Ni) (denoted as MBPO-CJ25) have been synthesized under mild hydrothermal conditions. Single-crystal X-ray diffraction analyses reveal that the three compounds possess isostructural three-dimensional (3D) open frameworks with one-dimensional 12-ring channels along the [001] direction. Notably, the structure can also be viewed as composed of metal phosphate layers $[M^{II}(PO_4)_2]^{4-}$ with Kagomé topology, which are further connected by $[B_3O_7(OH)]$ triborates, giving rise to a 3D open framework. The guest water molecules locate in the 12-ring channels. Partial Na^+ ions reside in the 10-ring side pockets within the wall of the 12-ring channels, and the other Na^+ ions and protonated water molecules locate in the 6-ring windows delimited by MO_6 and PO_4 polyhedra to compensate for the negative charges of the anionic framework. These compounds show a high thermal stability and are stable upon calcinations at ca. 500 °C. Ionic conductivities, due to the motion of Na^+ ions, are measured for these three compounds. They have similar activation energies of 1.13–1.25 eV and conductivities of 2.7×10^{-7}–9.9×10^{-7} S cm^{-1} at 300 °C. Magnetic measurements reveal that there are very weak antiferromagnetic interactions among the metal centers of the three compounds. Crystal data: MnBPO-CJ25, hexagonal, $P6_3/m$ (No. 176), a = 11.9683(5) Å, c = 12.1303(6) Å, and Z = 2; CoBPO-CJ25, hexagonal, $P6_3/m$ (No. 176), a = 11.7691(15) Å, c = 12.112(2) Å, and Z = 2; NiBPO-CJ25, hexagonal, $P6_3/m$ (No. 176), a = 11.7171(5) Å, c = 12.0759(7) Å, and Z = 2.

Introduction

Following the discovery of microporous aluminophosphates in 1982, the synthesis of new open-framework phosphate-based materials has attracted considerable attention for their potential applications in catalysis, adsorption, and separation.[1–3] Among these phosphate-based materials, the borophosphate compounds have shown fascinating structural chemistry and interesting properties in optical aspects.[4,5] So far, a large number of borophosphates with various anionic partial structures have been reported. Examples are known as $[NH_4]_4[Mn_9B_2(OH)_2(HPO_4)_4(PO_4)_6]$[6] with oligomeric units, $K[B_6PO_{10}(OH)_4]$[7] with one-dimensional (1D) loop-branched chains, $M^IM^{II}(H_2O)_2[BP_2O_8]\cdot H_2O$ (M^I = Na, K; M^{II} = Mg, Mn, Fe, Co, Ni, Zn)[8] with 1D infinite tetrahedral helical ribbons $[BP_2O_8]^{3-}$, $(C_2H_{10}N_2)[CoB_2P_3O_{12}(OH)]$[9] with two-dimensional (2D) layered structures, and $M[B_2P_2O_8(OH)]$ (M = Rb, Cs)[10] with three-dimensional (3D) open-framework structures. Besides, some zeotype borophosphates,[11–14] molybdenum borophosphate polyoxometalates,[15,16] and vanadium borophosphates[17–20] have also been reported.

As insight into the structural characters of borophosphates, most of them contain anionic partial structures built up from tetrahedral borate and phosphate groups. The B/P ratios of these compounds are usually equal to or less than 1.0. There

* To whom correspondence should be addressed. E-mail: jihong@mail.jlu.edu.cn.

(1) Cheetham, A. K.; Férey, G.; Loiseau, T. *Angew. Chem., Int. Ed.* **1999**, *38*, 3268 and references cited therein.
(2) Thomas, J. M.; Raja, R.; Sankar, G.; Bell, R. G. *Acc. Chem. Res.* **2001**, *34*, 191.
(3) Yu, J.; Xu, R. *Acc. Chem. Res.* **2003**, *36*, 481 and references cited therein.
(4) Kniep, R.; Engelhardt, H.; Hauf, C. *Chem. Mater.* **1998**, *10*, 2930 and references cited therein.
(5) Pan, S.; Wu, Y.; Fu, P.; Zhang, G.; Li, Z.; Du, C.; Chen, C. *Chem. Mater.* **2003**, *15*, 2218.
(6) Yang, M.; Yu, J.; Shi, L.; Chen, P.; Li, G.; Chen, Y.; Xu, R. *Chem. Mater.* **2006**, *18*, 476.
(7) Boy, I.; Kniep, R. *Z. Naturforsch., B* **1999**, *54B*, 895.
(8) Kniep, R.; Will, H. G.; Boy, I.; Röhr, C. *Angew. Chem., Int. Ed. Engl.* **1997**, *36*, 1013.
(9) Sevov, S. C. *Angew. Chem., Int. Ed. Engl.* **1996**, *35*, 2630.
(10) Hauf, C.; Kniep, R. *Z. Naturforsch., B* **1997**, *52B*, 1432.

10.1021/ic051916f CCC: $33.50 © 2006 American Chemical Society
Published on Web 04/01/2006

are only a few borophosphates containing B atoms in solely trigonal-planar[21−23] or both trigonal-planar and tetrahedral coordinations.[7,19,24−26] The latter generally possesses a B/P ratio larger than 1.0, which agrees with the rule that borophosphates with a molar ratio of B/P > 1 contain B atoms in both triangular and tetrahedral coordinations.[4]

On the other hand, transition-metal compounds with the Kagomé topology have been of considerable interest because of their novel magnetic properties, for example, geometric frustration.[27] To our knowledge, the borophosphates containing the Kagomé lattice have never been reported even though Kagomé structures are relatively abundant in inorganic compounds.[28−32]

Herein, we report three new isostructural transition-metal borophosphate compounds $Na_5(H_3O)\{M^{II}_3[B_3O_3(OH)]_3(PO_4)_6\}\cdot 2H_2O$ (M^{II} = Mn, Co, Ni) (denoted as MBPO-CJ25) with a new B/P ratio of 3/2. Their thermal stabilities, ionic conductivities, and magnetic properties are investigated in detail.

Experimental Section

Syntheses of MBPO-CJ25 (M = Mn, Co, Ni). The three title compounds can be prepared by a hydrothermal method. Typically, a mixture of H_3BO_3, $MCl_2\cdot nH_2O$ (M = Mn, Co, Ni; n = 4, 6, and 6 for Mn, Co, and Ni, respectively), $Na_2HPO_4\cdot 12H_2O$, and a HCl solution (18 wt %) with the molar composition of 16.2:1.0:6.0:2.0−3.0 was added into a 15-mL Teflon-lined stainless steel autoclave and heated at 200 °C for 5 days. The final product containing large single crystals in the form of a hexagonal prism was washed with hot water (50 °C) until the residual H_3BO_3 was completely removed, and then it was dried in air. Anal. Found (%) (calcd, wt %) for MnBPO-CJ25: Mn, 13.52 (13.77); B, 7.92 (8.13); P, 14.98 (15.52); Na, 10.11 (9.60). Found (%) (calcd, wt %) for CoBPO-CJ25: Co, 14.11 (14.62); B, 7.62 (8.05); P, 14.7 (15.37); Na, 10.3 (9.51). Found (%) (calcd, wt %) for NiBPO-CJ25: Ni, 13.91 (14.57); B, 7.67 (8.05); P, 14.80 (15.38); Na, 10.10 (9.51).

Single-Crystal Structure Determinations. Three suitable single crystals with dimensions 0.23 × 0.12 × 0.08, 0.32 × 0.28 × 0.24, and 0.20 × 0.20 × 0.15 mm were selected for single-crystal X-ray diffraction (XRD) analyses for MnBPO-CJ25, CoBPO-CJ25, and NiBPO-CJ25, respectively. The data were collected on a Siemens SMART CCD diffractometer using graphite-monochromated Mo Kα radiation (λ = 0.710 73 Å) at a temperature of 20 ± 2 °C. Data processing was accomplished with the SAINT processing program.[33]

The three structures were solved by direct methods and refined by full-matrix least-squares techniques with the *SHELXTL* crystallographic software package.[34] The Mn/Co/Ni, B, P, and O atoms could be unambiguously located. The Na^+ ions and Ow atoms were subsequently located from a difference Fourier map whose fractional occupancies were determined according to the charge balance as well as compositional and thermogravimetric analyses (TGA). All H atoms are not found. The H atom connected with the O(6) atom of the BO_3 group could not be added for its special position. Experimental details for crystal determinations of MBPO-CJ25 (M = Mn, Co, Ni) are listed in Table 1.

Characterizations. Powder XRD data were collected on a Siemens D5005 diffractometer with Cu Kα radiation (λ = 1.5418 Å). Inductively coupled plasma analysis was performed on a Perkin-Elmer Optima 3300Dv spectrometer. TGA studies were carried out on a NETZSCH STA 449C TGA/DTA analyzer in air with a heating rate of 10 °C min^{-1}.

Ionic Conductivities. Impedance measurements were performed by using a Solartron SI 1287 electrochemical interface and a Solartron SI 1260 impedance/gain-phase analyzer. Pellets with ca. 1.2-cm diameter and 1.5-mm thickness were prepared by cold pressing of the powder samples and were further sintered at 300 °C for 3 h to minimize the grain boundary effect. For a better contact, both sides of these pellets were coated with Ag powders and heated at 100 °C for 2 h. The scanning frequency ranged from 10^6 to 1.0 Hz, and the ac voltage applied was adjusted according to the resistance of each compound. The heating rate was kept at 2.5 °C min^{-1} from room temperature to 500 °C. The resistance of each compound was obtained from a circle fit of the impedance spectrum, and their conductivities were calculated by taking into account the thickness and area of the pellets.

Magnetic Measurements. Temperature-dependent magnetic susceptibility data were recorded on a Quantum-Design MPMS-XL SQUID magnetometer under an applied field of 1 kOe over the temperature range of 4−300 K.

Results and Discussion

Syntheses and Characterizations. Pure phases of MBPO-CJ25 (M = Mn, Co, Ni) can be easily prepared in the system of $16.2H_3BO_3-1.0MCl_2\cdot nH_2O-6.0Na_2HPO_4\cdot 12H_2O-(2.0-3.0)$HCl (M = Mn, Co, Ni; n = 4, 6, and 6 for Mn, Co, and Ni, respectively) at 200 °C for 5 days. Single-crystal XRD analyses reveal that they are isostructures with empirical formula $Na_5(H_3O)\{M^{II}_3[B_3O_3(OH)]_3(PO_4)_6\}\cdot 2H_2O$ (M = Mn, Co, Ni). It is found that the amount of HCl in the reaction mixture has a significant influence on the reaction products. Taking the CoBPO-CJ25 reaction system as an example,

(11) Kniep, R.; Schäfer, G.; Engelhardt, H.; Boy, I. *Angew. Chem., Int. Ed.* **1999**, *38*, 3642.
(12) Li, M.; Liu, W.; Ge, M.; Chen, H.; Yang, X.; Zhao, J. *Chem. Commun.* **2004**, 1272.
(13) Zhang, H.; Chen, Z.; Weng, L.; Zhou, Y.; Zhao, D. *Microporous Mesoporous Mater.* **2003**, *57*, 309.
(14) Yang, M.; Yu, J.; Chen, P.; Li, J.; Fang, Q.; Xu, R. *Microporous Mesoporous Mater.* **2005**, *87*, 124.
(15) Sassoye, C.; Norton, K.; Sevov, S. C. *Inorg. Chem.* **2003**, *42*, 1652.
(16) Dumas, E.; Debiemme-Chouvy, C.; Sevov, S. C. *J. Am. Chem. Soc.* **2002**, *6*, 908.
(17) Rijssenbeek, J. T.; Rose, D. J.; Haushalter, R. C.; Zubieta, J. *Angew. Chem., Int. Ed. Engl.* **1997**, *36*, 1008.
(18) Warren, C. J.; Haushalter, R. C.; Rose, D. J.; Zubieta, J. *Chem. Mater.* **1997**, *9*, 2694.
(19) Bontchev, R. P.; Do, J.; Jacobson, A. J. *Inorg. Chem.* **1999**, *38*, 2231.
(20) Zhao, Y.; Shi, Z.; Ding, S.; Bai, N.; Liu, W.; Zou, Y.; Zhu, G.; Zhang, P.; Mai, Z.; Pang, W. *Chem. Mater.* **2000**, *12*, 2550.
(21) Sevov, S. C.; Bontchev, R. P. *Inorg. Chem.* **1996**, *35*, 6910.
(22) Park, C. H.; Bluhm, K. *Z. Naturforsch., B* **1997**, *52B*, 102.
(23) Yilmaz, A.; Bu, X.; Kizilyalli, M.; Kniep, R.; Stucky, G. D. *J. Solid State Chem.* **2001**, *156*, 281.
(24) Hauf, C.; Kniep, R. *Z. Kristallogr.* **1996**, *211*, 707.
(25) Hauf, C.; Kniep, R. *Z. Kristallogr.—New Cryst. Struct.* **1997**, *212*, 313.
(26) Hauf, C.; Kniep, R. *Z. Kristallogr.* **1996**, *211*, 705.
(27) Greedan, J. E. *J. Mater. Chem.* **2001**, *11*, 37.
(28) Frunzke, J.; Hansen, T.; Harrison, A.; Lord, J. S.; Oakley, G. S.; Visser, D.; Wills, A. S. *J. Mater. Chem.* **2001**, *11*, 179.
(29) Grohol, D.; Nocera, D. G. *J. Am. Chem. Soc.* **2002**, *124*, 2640.
(30) Behera, J. N.; Paul, G.; Choudhury, A.; Rao, C. N. R. *Chem. Commun.* **2004**, 456.
(31) Bartlett, B. M.; Nocera, D. G. *J. Am. Chem. Soc.* **2005**, *127*, 8985.
(32) Ishiwata, S.; Wang, D.; Saito, T.; Takano, M. *Chem. Mater.* **2005**, *17*, 2789.
(33) *SMART* and *SAINT* (software packages); Siemens Analytical X-ray Instruments, Inc.: Madison, WI, 1996.
(34) *SHELXTL Program*, version 5.1; Siemens Industrial Automation, Inc.: Madison, WI, 1997.

Table 1. Crystal Data and Structural Refinement for MBPO-CJ25 (M = Mn, Co, Ni)[a]

compound	MnBPO-CJ25	CoBPO-CJ25	NiBPO-CJ25
empirical formula	$H_{10}B_9Mn_3Na_5O_{39}P_6$	$H_{10}B_9Co_3Na_5O_{39}P_6$	$H_{10}B_9Ni_3Na_5O_{39}P_6$
fw	1196.96	1208.93	1028.27
T (K)	293(2)	293(2)	293(2)
wavelength (Å)	0.710 73	0.710 73	0.710 73
cryst syst, space group	hexagonal, $P6/m$	hexagonal, $P6/m$	hexagonal, $P6_3m$
unit cell dimens			
a (Å)	11.9683(5)	11.7691(15)	11.7171(5)
b (Å)	11.9683(5)	11.7691(15)	11.7171(5)
c (Å)	12.1303(6)	12.112(2)	12.0759(7)
α (deg)	90	90	90
β (deg)	90	90	90
γ (deg)	120	120	120
V (Å^3)	1504.76(12)	1452.8(4)	1435.79(12)
Z, calcd density (Mg m^{-3})	2, 2.642	2, 2.764	2, 2.795
abs coeff (mm^{-1})	1.785	2.258	2.519
F(000)	1174	1186	1192
cryst size (mm^3)	0.23 × 0.12 × 0.08	0.32 × 0.28 × 0.24	0.20 × 0.20 × 0.15
θ range (deg) for data collection	1.96−28.23	2.00−28.10	2.01−28.25
limiting indices	$-15 \le h \le 10$, $-15 \le k \le 15$, $-14 \le l \le 16$	$-15 \le h \le 15$, $-14 \le k \le 9$, $-15 \le l \le 15$	$-15 \le h \le 15$, $-15 \le k \le 15$, $-9 \le l \le 15$
reflns collected/unique	10725/1301 [R(int) = 0.0806]	8727/1200 [R(int) = 0.0557]	9081/1212 [R(int) = 0.0396]
completeness to θ	28.23°, 100.0%	27°, 100.0%	27°, 100.0%
refinement method	full-matrix least squares on F^2	full-matrix least squares on F^2	full-matrix least squares on F^2
data/restraints/param	1301/0/107	1200/0/108	1212/0/108
GOF on F^2	1.214	1.329	1.343
final R indices [$I > 2\sigma(I)$]	R1 = 0.0608, wR2 = 0.1296	R1 = 0.0609, wR2 = 0.1396	R1 = 0.0571, wR2 = 0.1210
R indices (all data)	R1 = 0.0774, wR2 = 0.1336	R1 = 0.0610, wR2 = 0.1396	R1 = 0.0582, wR2 = 0.1214
largest diff peak and hole (e Å^{-3})	0.791 and −0.861	0.869 and −0.933	1.093 and −1.062

[a] $R1 = \sum[\Delta F/\sum(F_o)]$; $wR2 = (\sum[w(F_o^2 - F_c^2)])/\sum[w(F_o^2)^2]^{1/2}$, $w = 1/\sigma^2(F_o^2)$.

when the amount of HCl is increased from the initial 0.6 mL to 1.0 mL, while other reaction conditions are kept unchanged, $NaCo(H_2O)_2[BP_2O_8]\cdot H_2O$[8] related to the zeolite CZP topology is formed.

The powder XRD patterns of MBPO-CJ25 (M = Mn, Co, Ni) are shown in Figure S1 of the Supporting Information. The XRD patterns of the three compounds are in good agreement with their simulated ones on the basis of their single-crystal structural data, suggesting that they are pure phases.

The thermal properties of MBPO-CJ25 (M = Mn, Co, Ni) were studied by TGA, and their TGA curves are shown in Figure S2 of the Supporting Information. The TGA curve of CoBPO-CJ25 (dotted line) shows two stages of weight loss occurring from 260 to 570 °C. The first weight loss in a total of 4.8 wt % (calcd: 4.47 wt %) in the region of 260−530 °C corresponds to the loss of the water molecules in the pores. The second one of 2.6 wt % (calcd: 2.98 wt %) from 530 to 570 °C is ascribed to the removal of OH groups by dehydration. The TGA results of MnBPO-CJ25 and NiBPO-CJ25 are similar to those of CoBPO-CJ25, and their total weight losses are 7.2% (calcd: 7.51 wt %) and 7.0% (calcd: 7.45 wt %), respectively. XRD studies at different temperatures (Figure S1 of the Supporting Information) show that MnBPO-CJ25, CoBPO-CJ25, and NiBPO-CJ25 have a high thermal stability and that they can keep their structures intact upon calcinations at 450, 500, and 550 °C, respectively.

Crystal Structures of MBPO-CJ25 (M = Mn, Co, Ni). Single-crystal XRD analyses show that the MBPO-CJ25 (M = Mn, Co, Ni) compounds are isostructural and that all crystallize in the space group $P6_3/m$ (No. 176). The structure consists of a $\{M[B_3O_3(OH)](PO_4)_2\}^{2-}$ macroanionic framework with a new B/P ratio of 3/2, and the charge neutrality is achieved by Na^+ and H_3O^+ ions.

The asymmetric unit of CoBPO-CJ25 (Figure 1) contains

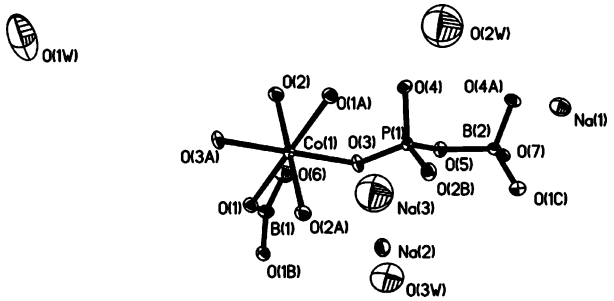

Figure 1. Thermal ellipsoid plots (50% probability) and atomic labeling schemes of CoBPO-CJ25.

two crystallographically distinct B sites. The B(1) atom located on the mirror plane shares two μ_3-O atoms with B(2) and Co(1) atoms [B(1)−O bond length: 1.363(6) Å], leaving a terminal hydroxyl group [B(1)−OH bond length: 1.385(11) Å] to form a trigonal plane. The B(2) atom is tetrahedrally coordinated and shares three μ_2-O atoms with two P atoms and one B(2) atom and also one μ_3-O atom with Co(1) and B(1) atoms [B(2)−O bond lengths: 1.419(7)−1.497(7) Å]. One unique P atom is tetrahedrally coordinated by O atoms and makes two P−O−Co bonds and two P−O−B bonds [P−O bond lengths: 1.514(4)−1.550(4) Å]. One crystallographically independent Co(1) atom locates at the inversion center and is bonded to four μ_2-O atoms [Co−μ_2-O_{av} bond length: 2.053(9) Å] and two μ_3-O atoms [Co−μ_3-O bond length: 2.264(4) Å], forming an octahedron. The asymmetric units of MnBPO-CJ25 and NiBPO-CJ25 are similar to that of CoBPO-CJ25, in which the Co atom is replaced by Mn and Ni atoms, respectively. The selected bond lengths and angles of MBPO-CJ25 (M = Mn, Co, Ni) are shown in Tables 2−4, respectively.

The linkage of one $B(1)O_2(OH)$ trigonal plane and two $B(2)O_4$ tetrahedra forms a $[B_3O_7(OH)]$ 3-ring motif, and then

Table 2. Selected Bond Lengths (Å) and Angles (deg) for MnBPO-CJ25[a]

Mn−O(3)#1	2.128(4)	O(3)−Mn(1)−O(1)#1	82.80(14)
Mn−O(3)	2.128(4)	O(2)#2−Mn(1)−O(1)#1	87.90(15)
Mn−O(2)#2	2.145(4)	O(2)#3−Mn(1)−O(1)#1	92.10(16)
Mn−O(2)#3	2.145(4)	O(3)#1−Mn(1)−O(1)	82.80(14)
Mn−O(1)	2.318(4)	O(3)−Mn(1)−O(1)	97.20(14)
Mn−O(1)#1	2.318(4)	O(2)#2−Mn(1)−O(1)	92.10(15)
P(1)−O(2)	1.513(4)	O(2)#3−Mn(1)−O(1)	87.90(15)
P(1)−O(3)	1.511(4)	O(1)#1−Mn(1)−O(1)	180.00(1)
P(1)−O(4)	1.556(4)	O(3)−P(1)−O(2)	113.4(2)
P(1)−O(5)	1.555(4)	O(3)−P(1)−O(5)	105.1(2)
B(1)−O(1)	1.358(6)	O(2)−P(1)−O(5)	112.4(2)
B(1)−O(1)#5	1.358(6)	O(3)−P(1)−O(4)	111.0(2)
B(1)−O(6)	1.389(11)	O(2)−P(1)−O(4)	109.9(3)
B(2)#3−O(1)	1.505(7)	O(5)−P(1)−O(4)	104.7(2)
B(2)#2−O(4)	1.476(8)	O(1)#5−B(1)−O(1)	122.9(7)
B(2)−O(5)	1.498(7)	O(1)#5−B(1)−O(6)	118.5(4)
B(2)#5−O(7)	1.428(7)	O(1)−B(1)−O(6)	118.5(4)
O(3)#1−Mn(1)−O(3)	180.000(1)	O(7)−B(2)−O(4)#6	108.8(5)
O(3)#1−Mn(1)−O(2)#2	88.95(16)	O(7)−B(2)−O(5)	109.5(5)
O(3)−Mn(1)−O(2)#2	91.05(16)	O(4)#6−B(2)−O(5)	107.9(5)
O(3)#1−Mn(1)−O(2)#3	91.05(16)	O(7)−B(2)−O(1)#4	110.9(5)
O(3)−Mn(1)−O(2)#3	88.95(16)	O(4)#6−B(2)−O(1)#4	110.2(5)
O(2)#2−Mn(1)−O(2)#3	180.0(3)	O(5)−B(2)−O(1)#4	109.4(5)
O(3)#1−Mn(1)−O(1)#1	97.20(14)		
Na(1)−O(7)	2.369(7)	Na(2)−O(2) (3×)	2.367(7)
Na(1)−O(6)	2.652(8)	Na(2)−O(6) (3×)	2.711(8)
Na(1)−O(5) (2×)	2.611(5)	Na(3)−O(2) (3×)	2.319(6)
Na(1)−O(3) (2×)	2.422(5)	Na(3)−O(3) (3×)	2.861(4)

[a] Symmetry transformations used to generate equivalent atoms: #1, $-x, -y+1, -z+1$; #2, $x-y, x, -z+1$; #3, $-x+y, -x+1, z$; #4, $-y+1, x-y+1, z$; #5, $x, y, -z+{}^3/_2$; #6, $y, -x+y, -z+1$.

Table 3. Selected Bond Lengths (Å) and Angles (deg) for CoBPO-CJ25[a]

Co(1)−O(3)#1	2.035(4)	O(3)−Co(1)−O(1)	95.50(15)
Co(1)−O(3)	2.035(4)	O(2)−Co(1)−O(1)	91.58(15)
Co(1)−O(2)	2.072(4)	O(2)#1−Co(1)−O(1)	88.42(15)
Co(1)−O(2)#1	2.072(4)	O(3)#1−Co(1)−O(1)#1	95.50(15)
Co(1)−O(1)	2.264(4)	O(3)−Co(1)−O(1)#1	84.50(15)
Co(1)−O(1)#1	2.264(4)	O(2)−Co(1)−O(1)#1	88.42(15)
P(1)−O(2)#2	1.514(4)	O(2)#1−Co(1)−O(1)#1	91.58(15)
P(1)−O(3)	1.515(4)	O(1)−Co(1)−O(1)#1	180.0(4)
P(1)−O(4)	1.550(4)	O(2)#2−P(1)−O(3)	113.7(2)
P(1)−O(2)	1.548(4)	O(2)#2−P(1)−O(2)	112.3(2)
B(1)−O(1)	1.363(6)	O(3)−P(1)−O(2)	104.4(2)
B(1)−O(1)#3	1.363(6)	O(2)#2−P(1)−O(4)	109.6(2)
B(1)−O(3)	1.385(11)	O(3)−P(1)−O(4)	111.1(2)
B(2)−O(1)#4	1.497(7)	O(2)−P(1)−O(4)	105.4(2)
B(2)−O(4)#2	1.476(7)	O(1)−B(1)−O(1)#3	123.4(7)
B(2)−O(5)	1.493(7)	O(1)−B(1)−O(3)	118.3(4)
B(2)−O(7)	1.419(7)	O(1)#3−B(1)−O(3)	118.3(4)
O(3)#1−Co(1)−O(3)	180.0(3)	O(7)−B(2)−O(4)#2	108.4(5)
O(3)#1−Co(1)−O(2)	87.97(16)	O(7)−B(2)−O(5)	109.5(5)
O(3)−Co(1)−O(2)	92.03(16)	O(4)#2−B(2)−O(5)	107.7(4)
O(3)#1−Co(1)−O(2)#1	92.03(16)	O(7)−B(2)−O(1)#4	111.6(5)
O(3)−Co(1)−O(2)#1	87.97(16)	O(4)#2−B(2)−O(1)#4	110.2(4)
O(2)−Co(1)−O(2)#1	180.0(2)	O(5)−B(2)−O(1)#4	109.4(4)
O(3)#1−Co(1)−O(1)	84.50(15)		
Na(1)−O(7)	2.361(7)	Na(2)−O(2) (3×)	2.361(6)
Na(1)−O(6)	2.550(8)	Na(2)−O(6) (3×)	2.660(8)
Na(1)−O(5) (2×)	2.548(5)	Na(3)−O(2) (3×)	2.326(6)
Na(1)−O(3) (2×)	2.459(5)	Na(3)−O(3) (3×)	2.778(4)

[a] Symmetry transformations used to generate equivalent atoms: #1, $-x+1, -y, -z$; #2, $y+1, -x+y+1, -z$; #3, $x, y, -z+{}^1/_2$; #4, $-y+1, x-y, z$.

these 3-ring motifs are further connected with PO_4 tetrahedra via vertex O atoms, forming 12-ring channels along the 6_3 screw axis in the [001] direction, in which water molecules locate. The pore sizes of the 12-ring motifs are 4.34 × 3.35 Å^2, 4.29 × 3.25 Å^2, and 4.28 × 3.22 Å^2 (the largest O···O distances) for MnBPO-CJ25, CoBPO-CJ25, and NiBPO-CJ25, respectively (Figure 2a). Within the wall of the 12-ring channel, 10-ring side pockets and $Na(1)^+$ ions exist

Table 4. Selected Bond Lengths (Å) and Angles (deg) for NiBPO-CJ25[a]

Ni(1)−O(3)	2.009(3)	O(3)#1−Ni(1)−O(1)#1	94.16(13)
Ni(1)−O(3)#1	2.009(3)	O(2)−Ni(1)−O(1)#1	88.53(14)
Ni(1)−O(2)	2.059(4)	O(2)#1−Ni(1)−O(1)#1	91.47(14)
Ni(1)−O(2)#1	2.059(4)	O(3)−Ni(1)−O(1)	94.16(13)
Ni(1)−O(1)#1	2.231(3)	O(3)#1−Ni(1)−O(1)	85.84(13)
Ni(1)−O(1)	2.231(3)	O(2)−Ni(1)−O(1)	91.47(14)
P(1)−O(2)#2	1.513(4)	O(2)#1−Ni(1)−O(1)	88.53(14)
P(1)−O(3)	1.512(4)	O(1)#1−Ni(1)−O(1)	180.00(18)
P(1)−O(4)	1.554(4)	O(3)−P(1)−O(2)#2	114.4(2)
P(1)−O(5)	1.551(4)	O(3)−P(1)−O(5)	104.2(2)
B(1)−O(1)#3	1.361(5)	O(2)#2−P(1)−O(5)	112.3(2)
B(1)−O(1)	1.361(5)	O(3)−P(1)−O(4)	110.9(2)
B(1)−O(6)	1.383(10)	O(2)#2−P(1)−O(4)	109.5(2)
B(2)−O(1)#1	1.504(6)	O(5)−P(1)−O(4)	105.0(2)
B(2)−O(4)	1.477(6)	O(1)#3−B(1)−O(1)	123.5(7)
B(2)−O(5)#4	1.488(6)	O(1)#3−B(1)−O(6)	118.3(3)
B(2)−O(7)	1.412(6)	O(1)−B(1)−O(6)	118.3(3)
O(3)−Ni(1)−O(3)#1	180.0	O(7)−B(2)−O(4)	108.6(4)
O(3)−Ni(1)−O(2)	92.42(15)	O(7)−B(2)−O(5)#4	109.9(4)
O(3)#1−Ni(1)−O(2)	87.58(15)	O(4)−B(2)−O(5)#4	107.5(4)
O(3)−Ni(1)−O(2)#1	87.58(15)	O(7)−B(2)−O(1)#1	111.2(4)
O(3)#1−Ni(1)−O(2)#1	92.42(15)	O(4)−B(2)−O(1)#1	110.2(4)
O(2)−Ni(1)−O(2)#1	180.00(19)	O(5)#4−B(2)−O(1)#1	109.4(4)
O(3)−Ni(1)−O(1)#1	85.84(13)		
Na(1)−O(7)	2.363(6)	Na(2)−O(2) (3×)	2.347(6)
Na(1)−O(6)	2.519(7)	Na(2)−O(6) (3×)	2.647(7)
Na(1)−O(5) (2×)	2.525(5)	Na(3)−O(2) (3×)	2.326(6)
Na(1)−O(3) (2×)	2.460(4)	Na(3)−O(3) (3×)	2.752(4)

[a] Symmetry transformations used to generate equivalent atoms: #1, $-x+2, -y+1, -z$; #2, $y+1, -x+y+1, -z$; #3, $x, y, -z+{}^1/_2$; #4, $x-y, x-1, -z$.

(Figure 2b). These hexagonally arrayed 12-ring channels are connected by MO_6 octahedra to construct the 3D open-framework structure of MBPO-CJ25, giving rise to 6-ring windows consisting of MO_6 and PO_4 polyhedra (Figure 3a). Interestingly, the linkages of MO_6 octahedra and PO_4 tetrahedra result in a 2D layer structure exhibiting a famous Kagomé lattice (the inset of Figure 3a). Triborates $[B_3O_7(OH)]$ act as pillars between these 2D layers to construct the 3D structure of MBPO-CJ25 (Figure 3b).

The negative charges of the anionic frameworks are compensated for by Na^+ and H_3O^+ ions. Na(1) locates in the 10-ring side pockets within the wall of 12-ring channels (Figure 2b), and Na(2), Na(3), and H_3O^+ ions lie in the 6-ring tunnels delimited by MO_6 and PO_4 polyhedra (Figure 3). Figure S3 of the Supporting Information shows the coordination environments of all of the Na^+ ions. All of the Na^+ ions are coordinated by six O atoms, and the Na−O distances for the three compounds are listed in Tables 2−4, respectively, which are comparable to those in $NaZn(H_2O)_2[BP_2O_8]\cdot H_2O$.[35]

So far, only three alkali-metal borophosphates, $K[B_6PO_{10}(OH)_4]$ (B/P = 6),[7] $K_3[B_5PO_{10}(OH)_3]$ (B/P = 5),[24] and $Li[B_3PO_6(OH)_3]$ (B/P = 3),[25] and one ammonium borophosphate, $(NH_4)_2[B_3PO_7(OH)_2]$ (B/P = 3),[26] have been known to possess B/P ratios higher than 1. The MBPO-CJ25 (M = Mn, Co, Ni) compounds represent the first transition-metal borophosphates with high B contents (B/P = 3/2). The remarkable feature of these structures with B/P ratios higher than unity is the presence of trigonal-planar borate groups, which are exclusively connected with borate species, forming

(35) Boy, I.; Stowasser, F.; Schäfer, G.; Kniep, R. *Chem.—Eur. J.* **2001**, *7*, 834.

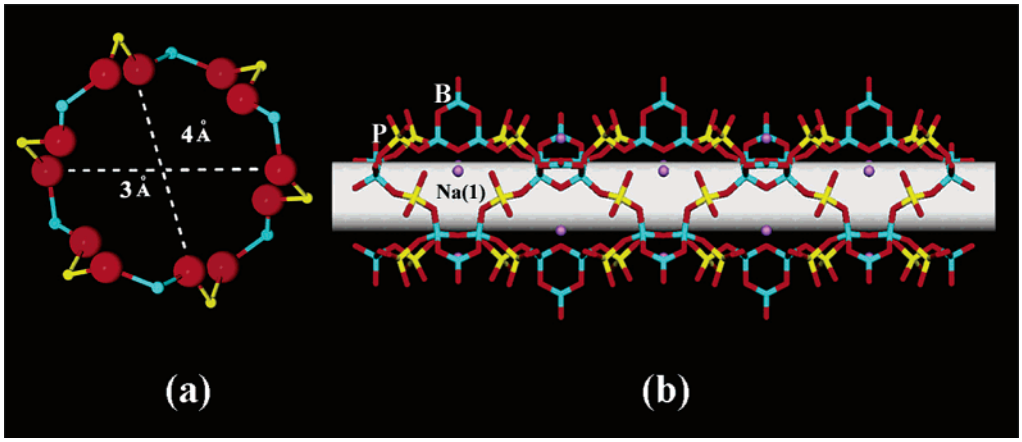

Figure 2. (a) 12-ring window viewed along the *c* axis. (b) 10-ring side pockets and Na(1) atoms within the wall of the 12-ring channel viewed along the *a* axis. Color code: P, yellow; B, sky blue; Na, purple; O, red.

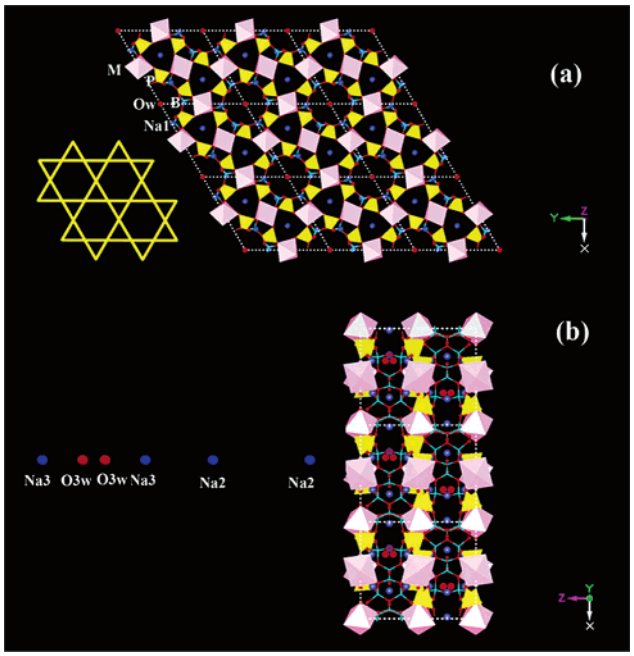

Figure 3. (a) Open framework of MBPO-CJ25 viewed along the *c* axis. The left inset is a schematic presentation of the Kagomé lattice. (b) Open framework of MBPO-CJ25 viewed along the *b* axis. The left inset is the arrangement of Na^+ and H_3O^+ ions inside the 6-ring window. Color code: M, pink; P, yellow; B, sky blue; Na, blue; O, red.

3-ring motifs. Except for one 0D $[N_2C_6H_{14}]_2VO(PO_3OH)_4(B_3O_3OH)\cdot 4H_2O$,[19] whose structure holds the cluster-like borophosphate anionic parts with 3-ring motifs and a B/P ratio of 3/4, the MBPO-CJ25 (M = Mn, Co, Ni) compounds are the first transition-metal borophosphates containing 1D anionic channel structures and 3-ring motifs.

Ionic Conductivities. The impedance measurements of MBPO-CJ25 (M = Mn, Co, Ni) were performed on sintered pellets. The plots of the bulk conductivity [log(σT)] vs reciprocal temperature (1000/T) for these three compounds are shown in Figure 4. The data are well-fitted to the Arrhenius expression $\sigma T = \sigma_0 \exp(-E/KT)$, where σ_0 is a preexponential factor, E is the activation energy, and K is the Boltzmann constant. The E and σ_0 parameters, together with the conductivities at 300 °C, are outlined in Table 5. Their E values fall in the range of 1.13−1.25 eV, and conductivities (σ) at 300 °C change from 2.7×10^{-7} to 9.9×0^{-7} S cm^{-1}.

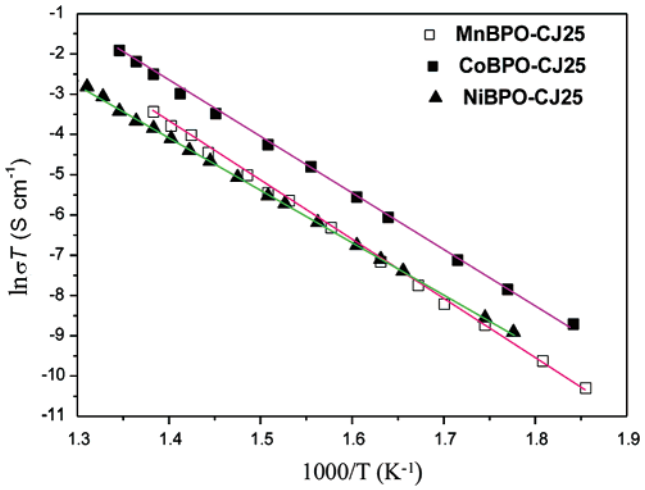

Figure 4. Plots of the bulk conductivity vs 1000/T for the Mn, Co, and Ni compounds. The straight lines are the best fits to the equation $\sigma T = \sigma_0 \exp(-E/KT)$.

Table 5. Activation Energies (E), Preexponential Factors (σ_0), and Ionic Conductivities at 300 °C (σ_{300}) for MBPO-CJ25 (M = Mn, Co, Ni)

compound	E (eV)	σ_0 (S cm^{-1})	σ_{300} (S cm^{-1})
MnBPO-CJ25	1.25	1.50×10^7	2.7×10^{-7}
CoBPO-CJ25	1.19	1.47×10^7	9.9×10^{-7}
NiBPO-CJ25	1.13	1.51×10^7	3.3×10^{-7}

These data are comparable to those of reported $Na_4Ni_5(PO_4)_2(P_2O_7)_2$[36] and $Na_4M^{II}_3(PO_4)_2(P_2O_7)$[37] (M = Mn, Co, Ni). Compared with the good Na^+ ion conductors, such as NASICON, related NASICON compounds, and β-alumina,[38−42] however, the lower conductivity and higher activation energy of MBPO-CJ25 indicate that Na^+ ions in these compounds move with difficulty.

(36) Sanz, F.; Parada, C.; Rojo, J. M.; Ruiz-Valero, C. *Chem. Mater.* **1999**, *11*, 2673.
(37) Sanz, F.; Parada, C.; Rojo, J. M.; Ruiz-Valero, C. *Chem. Mater.* **2001**, *13*, 1334.
(38) Hong, H. Y. P. *Mater. Res. Bull.* **1976**, *11*, 173.
(39) Goodenough, J. B.; Hong, H. Y. P.; Kafalas, J. A. *Mater. Res. Bull.* **1976**, *11*, 203.
(40) Winand, J. M.; Pulmont, A.; Tarte, P. *J. Mater. Sci.* **1990**, *25*, 4008.
(41) Collongues, R.; Kahn, A.; Michel, D. *Annu. Rev. Mater. Sci.* **1979**, *9*, 123.
(42) Martínez-Juarez, A.; Pecharromán, C.; Iglesias, J. E.; Rojo, J. M. *J. Phys. Chem. B* **1998**, *102*, 372.

Magnetic Properties. The temperature dependences of the magnetic susceptibilities of MBPO-CJ25 (M = Mn, Co, Ni) were recorded at an applied magnetic field of 1000 Oe over the temperature range of 4−300 K. Figure S4 of the Supporting Information shows the plots of χ_m and $1/\chi_m$ vs T of the three compounds, respectively. The susceptibility obeys the Curie−Weiss rule [$\chi_m = C/(T - \theta)$] over a wide range of temperatures (4−300 K) for MnBPO-CJ25. The effective magnetic moment per Mn^{2+} calculated from the derived Curie constant is 6.04 μ_B. The negative Weiss constant, $\theta = -2.4$ K, implies a weak antiferromagnetic interaction between Mn^{2+} ions. As insight into the structure of MnBPO-CJ25 based on the magnetic point, although the Mn^{2+} ions are positioned at the vertexes of the triangles, they are connected through PO_4 groups within the Kagomé layers and by the $[B_3O_7(OH)]$ triborates between the Kagomé layers. Correspondingly, the Mn···Mn distances are ca. 5.984 and 6.065 Å, respectively. Different from a concentrated Kagomé structure with a spin-frustration phenomenon,[27] the absence of spin frustration in MnBPO-CJ25 may be due to the larger distance between the adjacent metal atoms. The magnetic measurement results of CoBPO-CJ25 and NiBPO-CJ25 are similar to those of MnBPO-CJ25. The negative Weiss constants, $\theta = -15.2$ K for CoBPO-CJ25 and $\theta = -5.5$ K for NiBPO-CJ25, suggest a very weak antiferromagnetic exchange ordering occurring among the metallic centers. The room-temperature effective magnetic moments derived from the measurements, i.e., 5.15 μ_B per Co^{2+} ion and 3.46 μ_B per Ni^{2+} ion, are higher than the expected spin-only values. This is attributed to the orbital contribution of Mn^{2+} ions.[43,44]

Conclusions

Three new isostructural transition-metal borophosphates MBPO-CJ25 (M = Mn, Co, Ni) with a new B/P ratio of 3/2 have been prepared by the hydrothermal method. These compounds are the first examples containing 1D 12-ring-channel anionic partial structures with both BO_3 and BO_4 groups. They are also the first borophosphates containing a 2D Kagomé lattic built up from the connection of PO_4 and MO_6 polyhedra. The ionic conductivity measurements show that the three compounds have similar activation energies and conductivities at 300 °C, suggesting that Na^+ ions can move with difficulty. The magnetic studies show that the three compounds are all weak antiferromagnets. The successful preparation of MBPO-CJ25 (M = Mn, Co, Ni) will promote the further development of new open-framework transition-metal borophosphate materials with interesting structural architectures and properties.

Acknowledgment. This work is supported by the National Natural Science Foundation of China.

Supporting Information Available: The crystallographic data in CIF format, X-ray powder patterns, TGA curves, coordination environments of Na atoms, and the χ_m vs T and $1/\chi_m$ vs T plots for MBPO-CJ25 (M = Mn, Co, Ni). This material is available free of charge via the Internet at http://pubs.acs.org.

IC051916F

(43) Carlin, R. L. *Magnetochemistry*; Springer-Verlag: Berlin, 1986.
(44) Chang, W.; Chiang, R.; Jiang, Y.; Wang, S.; Lee, S.; Lii, K. *Inorg. Chem.* **2004**, *43*, 2564.